

24 **1. Introduction**

25 In China, the total energy consumption was 4.86 billion tons of standard coal in 2019, and coal
26 consumption accounted for 57.7% (Society, 2020). Confined by the structure of energy resources,
27 coal continues to contribute a significant part for China's energy strategy for a long term. However,
28 the utilization of coal causes lots of environmental problems, among which nitrogen oxide (NO_x) is
29 one of the major pollutants responsible for the smog and acid rain formation. Developing clean coal
30 usage technologies with high efficiency and low NO_x emission is becoming more and more urgent
31 under the stringent emission standards for air pollutants. In the last several decades, many NO_x
32 reduction and removal technologies, such as low NO_x burner (Song et al., 2020), air staging (Wang,
33 Y. et al., 2020), reburning (Chernetskiy et al., 2018), and moderate or intense low-oxygen dilution
34 (MILD) combustion have been developed. However, ultra-low NO_x emission and high efficiency
35 combustion technologies remain required, with increasingly stringent emission standards for coal
36 combustion.

37 Based on the understanding of NO_x formation and destruction, a promising method, pulverized
38 coal (PC) preheating-combustion technology, was proposed. PC was preheated before entered the
39 combustion zone. During the preheating stage, volatile in coal would easily release and promote the
40 conversion of most volatile-N into N_2 in an oxygen-deficient environment (Taniguchi et al., 2012;
41 Wu et al., 2019). All-Russian Thermal Energy Institute (Rabovitser et al., 2003) first proposed and
42 investigated the NO_x emission of PC preheating technology by means of natural gas combustion-
43 supporting. The NO_x reduction efficiency of 80% and 60% were achieved when PC was preheated
44 to 1083 K and 863 K respectively. Similarly, the Gas Technology Institute conducted above research
45 on a 0.88 MW test furnace and reached similar conclusions (Bryan et al., 2005; Rabovitser et al.,
46 2007). Recently, Liu et al. (Liu et al., 2015a; Liu et al., 2014; Liu et al., 2015b) also investigated the

47 effect of PC preheating on NO_x emission characteristics in a 35 kW furnace in detail and found that
48 NO emission could be reduced by 74% and 67% for bituminous coals with volatile content of 34.4%
49 and 38.0% (with preheating temperature at 1073 K). Liu et al. (Liu et al., 2015a) also pointed out
50 that PC preheating could be incorporated with other de-NO_x technologies such as air staging and
51 MILD combustion. Besides, series of self-preheating swirl burners with multi-air staging were
52 designed and evaluated in the same drop tube furnace. About 70% of NO_x emission was reduced
53 and the final NO emission could reach 217 mg·m⁻³ (Zhu et al., 2021).

54 Meanwhile, a method to achieve preheated PC through a circulating fluidized bed (CFB) has
55 been proposed and adopted by the Academy of Chinese, which shows the ability to implement stable
56 PC combustion, high burnout efficiency and low NO emission. Ouyang (Ouyang et al., 2020;
57 Ouyang et al., 2018a; Ouyang et al., 2018c; Ouyang et al., 2013) found that the NO_x emission
58 concentration could be reduced to 372, 295, 259 and 265 mg·m⁻³ with preheating temperature at
59 1073, 1123, 1173 and 1223 K, respectively. After further coupled with flameless combustion
60 technology (Liu et al., 2018; Ouyang et al., 2018b; Zhu et al., 2018), the NO_x emission value could
61 be further reduced to 108 mg·m⁻³ (6% O₂). Above studies demonstrated the potential advantages of
62 preheating-combustion technology to reduce NO_x. Besides, Ouyang et al. (Ouyang et al., 2013)
63 suggested that raising preheating temperature benefitted the corresponding NO reduction efficiency
64 and combustion performance of low volatile PC.

65 Raising the temperature can induce more coal-N to release and convert under oxygen deficient
66 atmosphere (LeBlanc et al., 2017). Thus, more NO precursor prefers to form N₂, which can
67 significantly avoid the NO formation during following combustion process (Bai et al., 2014;
68 Taniguchi et al., 2011; Wang, S. et al., 2020). However, aforementioned studies were limited by low

69 preheating temperature, which was usually lower than 1173 K, especially for that preheat PC with
70 CFB. There has not been a detailed research on the NO_x reduction potential of preheating-
71 combustion technology with higher preheating temperature. In this paper, two electric heating drop
72 tube furnaces were connected in series to provide a high-temperature preheating and combustion
73 environment respectively. Higher preheating temperature was chosen to extend the preheating-
74 combustion to a higher temperature level and reveal the NO reduction potential under higher
75 preheating temperature. The effects of preheating temperature, residence time and excess air ratio
76 (EAR) in preheating zone on NO formation were evaluated to extend PC preheating technology to
77 a higher preheating temperature. Moreover, the migration and transformation characteristics of coal-
78 N were explored through kinetic modeling to reveal the mechanism of preheating-combustion
79 technology to reduce NO with higher preheating temperatures.

80 2. Experiments

81 2.1 Fuel

82 Table.1 Fuel Analyses of Huangling (HL) Bituminous Coal

Parameter	Ultimate Analysis/%					Proximate Analysis/%			
	C _d	H _d	N _d	O _d	S _d	M _{ad}	A _d	V _{daf}	FC _{ad}
Value	70.65	4.39	0.86	12.15	0.49	3.80	11.46	37.69	53.08

83 _d: dry basis, _{ad}: air dried basis, _{daf}: dry and ash-free basis.

84 In this experiment, Huangling (HL) bituminous coal, characteristic by high volatile content up
85 to 37.69%, was chosen. High volatile content favors the release of coal-N during devolatilization.
86 Therefore, more nitrogen-containing compounds tend to migrate into gas phase and convert in
87 oxygen-deficient condition during preheating, which would benefit NO reduction and give a better
88 insight into the NO_x reduction potential of preheating-combustion technology. The coal sample was

89 sieved to 75~90 μm and dried at 378 K for 24 hours before the preheating-combustion experiments.

90 The coal properties were summarized in Table 1.

91 2.2 Experimental apparatus

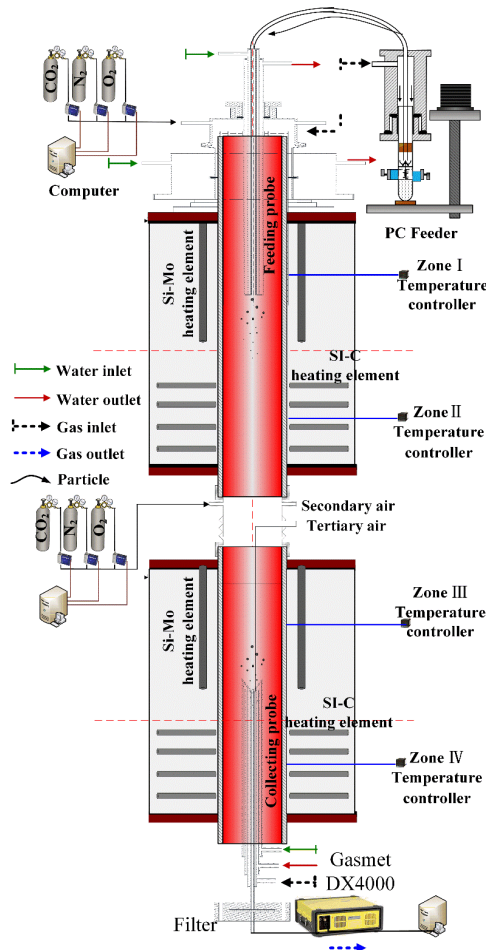
92 As shown in Fig.1, the PC preheating-combustion process was conducted in two connected

93 electric heating DTF. The furnace can achieve the maximum temperature of 1873 K. A corundum

94 tube, with an inner diameter of 51 mm and length of 1200 mm, was fixed in the center of the furnace

95 to act as reactor. By controlling the interior temperature of the upper furnace for preheating the PC,

96 the inner temperature of the bottom furnace was adjusted for burning the preheated product.



97

98 Fig.1 Schematic diagram of PC preheating-combustion system

99 In this work, two DTFs were used and each atmosphere could be controlled separately.

100 Therefore, the preheating zone and combustion chamber have their own EAR and temperature,

101 using EAR_p , T_p and EAR_c , T_c to denote, respectively. EAR was defined as Eq.1.

$$102 \quad EAR = \frac{\text{amount of oxygen supplied}}{\text{amount of oxygen required for stoichiometry}} \quad (\text{Eq.1})$$

103 During experiment process, the preheating oxidizer was injected from the upper furnace,
104 whereas the oxidizer for combustion of preheated fuel was injected from the connector between
105 those two DTFs. Each flow rate was controlled according to the PC feeding rate and EAR. The
106 overall EAR was kept constant at 1.2, i.e., $EAR_p + EAR_c = 1.2$, which was the same as that in actual
107 boiler. The experimental system consisted of some auxiliaries, including PC feeder, gas distributor,
108 particle filter and flue gas analyzer. Detailed information on each auxiliary and calculation method
109 of coal-N conversion can be found in our previous paper (Wang, S. et al., 2020).

110

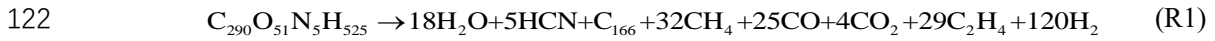
Table.2 Experimental conditions

Parameters	Values
T_p/K	1373,1473,1573
T_c/K	1273,1473
EAR_p	0,0.1,0.2,0.4,0.6,0.8,1.2
Residence time/s	0.1,0.15,0.185,0.225,0.3,0.45
EAR_p+EAR_c	1.2
Overall residence time/s	~1.0

111 2.3 Kinetic modeling

112 In order to quantitatively investigate the migration and conversion of coal-N, preheating
113 combustion process is modeled using two connected plug flow reactors (PFR) with Chemkin-Pro.
114 Two gas inlets were required, namely Inlet I (representing the devolatilization products, char, and
115 oxidizer for preheating stage) and Inlet II (oxidizer for preheated products). The detailed kinetic
116 mechanism used herein was a combination of the heterogeneous mechanisms developed by

117 Hashemi et al. (Hashemi et al., 2011) and the homogeneous mechanisms developed by Glarborg et
 118 al. (Glarborg et al., 2018). The heterogeneous mechanisms were used to simulate the combustion of
 119 char and conversion of char-N, and the homogeneous mechanisms was used to simulate the
 120 conversion of gaseous species. Actually, Hashemi also propose a single step reaction, as shown in
 121 R1, to handle the devolatilization of PC (Hashemi et al., 2011).



123 However, this single reaction can't fully capture the effect of devolatilization temperature on
 124 the proportion of volatile and char, especially the release of coal-N into gas phase. A modification
 125 must consider the influence of preheating temperature. Therefore, the chemical percolation
 126 devolatilization (CPD) model (Tian et al., 2001) was used here to predict the composition of volatile
 127 and the release of coal-N. The results of CPD prediction were taken as input condition for above-
 128 mentioned kinetic modeling. The assumed chemical formula of char, C_{412}N_5 , proposed by Hashemi
 129 (Hashemi et al., 2011), is adopted. We keep using the same formula even though there are some
 130 slightly difference regarding to the ratio of N/C between the coal used here and the coal used by
 131 Hashemi (Hashemi et al., 2011). Since what we focus is the conversion ratio of coal-N to NO rather
 132 than the burnout of char. Therefore, the amount of char for simulation input is decide according to
 133 the coal-N balance. Input of char is calculated according to Eq.2. The detailed input parameters for
 134 Chemkin-Pro can be found in Supplementary file.

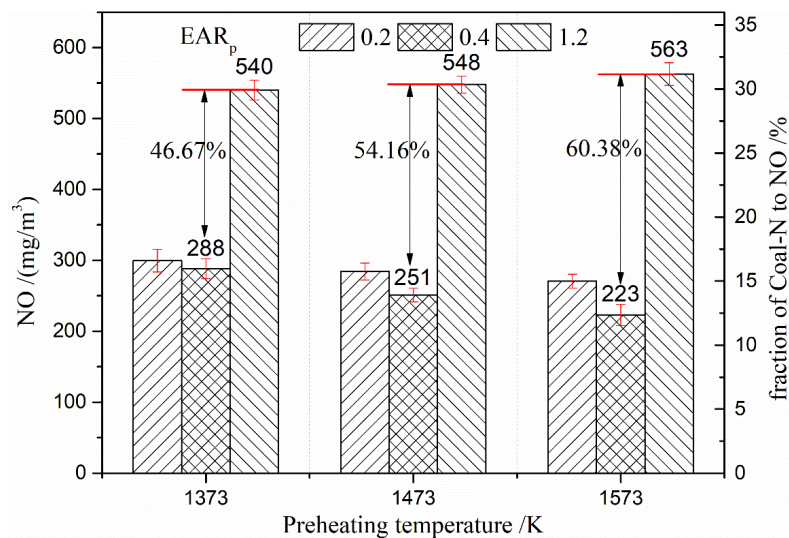
$$135 \quad n_{\text{char}} = \frac{m_{\text{coal}} \times N_{\text{d}} \times N_{\text{char}}}{M \cdot 5} \quad (\text{Eq.2})$$

136 where n_{char} denotes the mole of char for calculation input; m_{coal} is the feeding mass of PC; N_{d} is the
 137 nitrogen content in coal as shown in table 1; N_{char} is the fraction of coal-N remain in char after
 138 devolatilization during modeling process; M is the molar mass of nitrogen, which is 14 here.

139 **3. Results and discussion**

140 **3.1 Effect of preheating temperatures on NO emission**

141 Fig.2 shows the effects of preheating temperatures on NO emission under different EAR_p .
142 Compared with conventional PC combustion ($EAR_p=1.2$), preheating was observed to pose an
143 extraordinary impact on NO emissions ($EAR_p=0.2, 0.4$). NO emission was reduced significantly
144 after preheating, confirming the excellent NO reduction potential of PC preheating-combustion
145 technology. Furthermore, as the preheating temperature increased, the NO emission decreased. For
146 instance, the NO emission decreased from 288 to 223 $mg \cdot m^{-3}$ with an increase in the preheating
147 temperature from 1373 to 1573 K ($EAR_p = 0.4$). Besides, NO was reduced by 252, 297, and 350
148 $mg \cdot m^{-3}$ when PC was preheated to 1373, 1473, and 1573 K, respectively. The difference in NO
149 emission under conditions with and without preheating became more pronounced with elevated
150 preheating temperatures. The corresponding performance of the NO reduction was improved from
151 46.67% to 60.38%, and the post-combustion processing of flue gas would benefit greatly in meeting
152 the NO_x emission requirements.



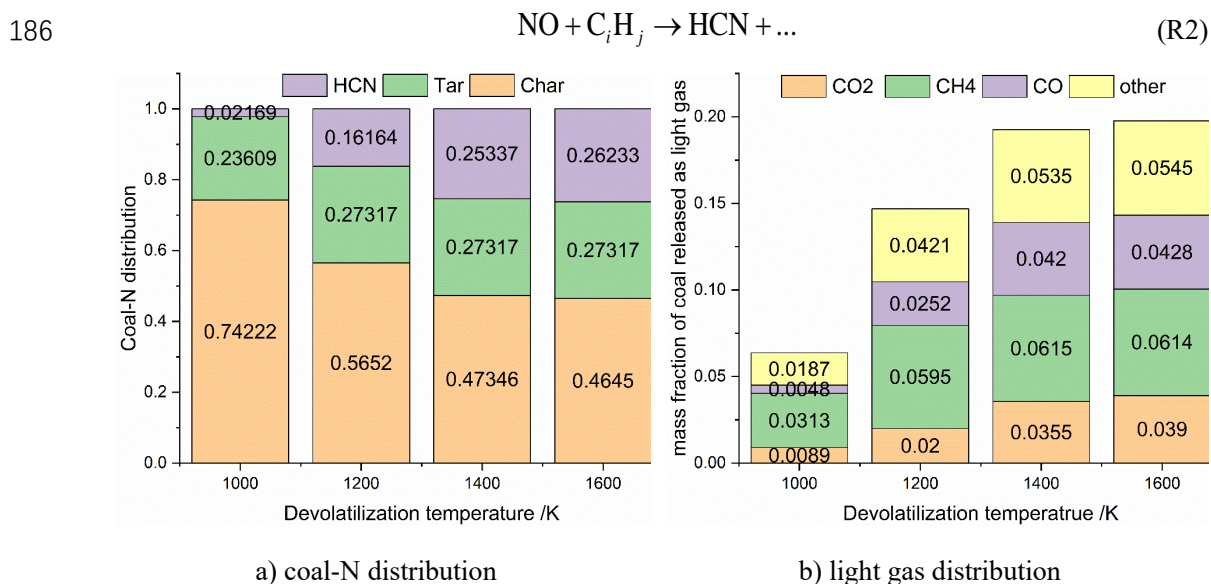
153 Fig.2 Effects of preheating temperatures on NO emission under different EAR_p .
154

155 In this study, all experimental temperatures for both preheating and combustion were less than

156 1773 K. Consequently, the contribution of thermal NO to the final NO emissions would be
157 significantly low (Glarborg et al., 2003). The measured NO was mainly derived from the oxidation
158 of coal-N. Thus, subsequent analysis on the effects of preheating temperature mainly focused on the
159 conversion of coal-N. Based on information in the literature, temperature is thought to have a
160 significant influence on the splitting of coal-N into volatiles and char (Niksa, 2019a, b). The effect
161 of the preheating temperature on coal-N distribution can be predicted using CPD model. The results
162 are shown in Fig.3a. Around a quarter of coal-N at the preheating temperature of 1000 K was
163 released as volatile-N, while it reached more than a half at the preheating temperature of 1600 K.
164 Similar results that the nitrogen fraction released as volatile increased dramatically with increased
165 temperature were reported in the literature (Niksa, 2019a, b). Under high preheating temperatures
166 and fuel-rich atmospheres, more coal-N tends to be released and converted to N₂ rather than to NO
167 in preheating stage (Liu et al., 2014), thus enhancing the potential for NO reduction with PC
168 combustion (Niu et al., 2017). This conclusion is consistent with the results of He et al. (He et al.,
169 2004), who indicated that the greater the proportion of volatile-N to coal-N, the more fuel nitrogen
170 can be converted to N₂. By contrast, during the conventional PC combustion process without
171 preheating, coal-N was released and converted under fuel-lean condition. Thus, temperature would
172 pose reverse impact on NO formation. A higher temperature accelerated the volatile-N oxidation
173 and the NO formation under an oxidizing atmosphere, whereas a higher temperature favors the NO
174 reduction under a reducing atmosphere. Thereby, NO emission for that with and without preheating
175 differed more pronounced at higher preheating temperatures.

176 In a fuel-rich zone, hydrocarbon (C_iH_j) also plays as a major factor in NO reduction, especially
177 under high temperatures (Taniguchi et al., 2010). The reaction between NO and C_iH_j could be

178 expressed in a simplified global reaction, as shown in R2. Yields of C_iH_j from coal preheating have
 179 also been predicted using the CPD model (Tian et al., 2001). Fig.3b specifically indicated that the
 180 concentration of C_iH_j increased with the raised temperature. Yields of C_iH_j at 1600 K were almost
 181 twice that of 1000 K. The ‘other’ in Fig.3 b) means the hydrocarbon species other than CH_4 in
 182 volatile, including C_2H_4 , C_2H_6 . Besides, temperature would not only accelerate the yields of C_iH_j
 183 during devolatilization but also the reaction rate between C_iH_j and NO (Hu et al., 2019; Taniguchi
 184 et al., 2010). Finally, high preheating temperature promoted the conversion of NO_x precursor to N_2 ,
 185 thus reducing the final NO emission.

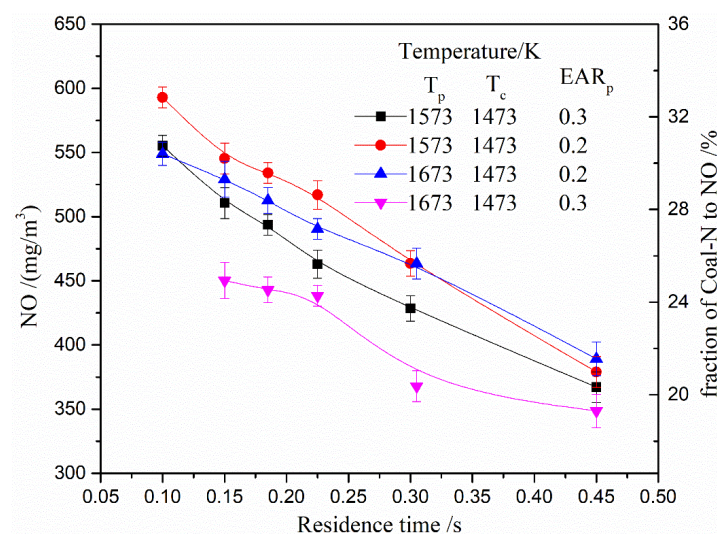


187 Fig.3 Effects of preheating temperatures on devolatilization products predicted by the CPD model.

188 3.2 Effects of residence times in preheating zone on NO emission

189 Fig.4 shows the effects of residence times in preheating chamber on NO emission under
 190 different preheating and combustion temperatures. It was observed that the measured NO showed a
 191 remarkable decrease as the residence time increase. The NO dropped from $593 \text{ mg}\cdot\text{m}^{-3}$ to less than
 192 $379 \text{ mg}\cdot\text{m}^{-3}$ as the residence time increased from 0.1 s to 0.45 s ($EAR_p=0.2$, $T_p=1573 \text{ K}$ and $T_c=1473$
 193 K). This meant that the preheating time for an actual boiler should be prolonged as much as possible

194 to reduce NO_x formation during the preheating-combustion process. However, it should be noted
 195 that, in our experiment, the curve became flat when the residence time continued to increase after a
 196 rapid decline at T_p=1673 K, T_c=1473 K and EAR_p=0.3. This indicated that a NO reduction threshold
 197 existed when the residence time was sufficiently long. This threshold value appeared earlier with
 198 the elevated preheating temperature and EAR_p.

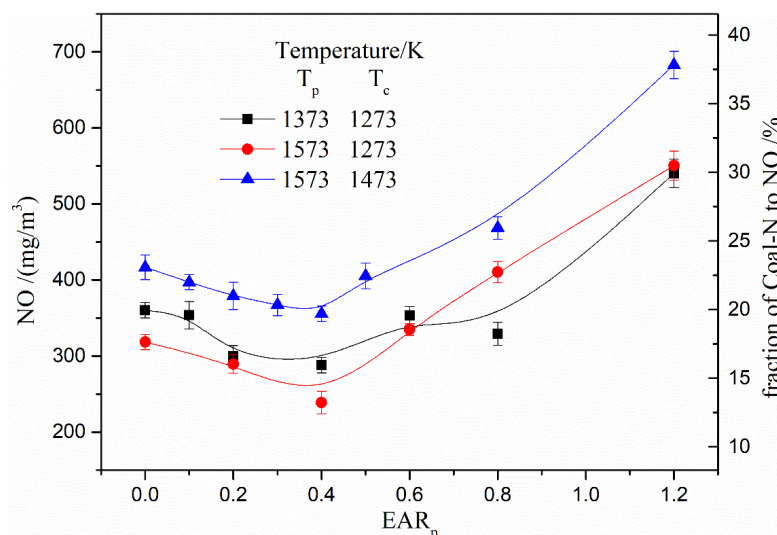


199
 200 Fig.4 Effects of residence times in the preheating zone on NO emission.

201 NO formation from the combustion of preheated PC can be attributed to two main sources: the
 202 homogeneous reaction of volatile-N and the heterogeneous reaction of char-N (Molina et al., 2009).
 203 This study therefore centered on two aspects of the reduction in NO formation with an improvement
 204 in preheating time: the N₂ formation from volatile N and the association of char-N and other
 205 nitrogen-containing gasses to mitigate the NO formation during char combustion. Attributing to
 206 long residence time in preheating zone, the gas phase reaction became more complete, resulted in
 207 more formation of N₂ and less existence of reactive nitrogen containing species (such as HCN) in
 208 outlet of preheating chamber. Therefore, NO emission from oxidation of preheated gas dropped
 209 down. Besides, some researchers have shown that HCN and its precursors could interact
 210 considerably with char to form N₂ (Molina et al., 2009; Wu et al., 2019). With a prolonged residence

211 time in oxygen deficient atmosphere, nitrogen containing sites on the char surface may have greater
 212 potential to react with nitrogen containing gases, such as HCN to convert into N_2 . This suggested
 213 that with prolonged preheating time, a portion of char-N continues to interact with nitrogen
 214 containing species and convert to N_2 , resulted in less nitrogen exists in char (Ma et al., 2019; Ulusoy
 215 et al., 2019). Consequently, less char-N reduces the potential of NO formation during the oxidation
 216 of preheated char, benefiting the final reduction of NO emission during preheating-combustion
 217 process.

218 3.3 Effects of the stoichiometric ratio in the preheating zone on NO emission



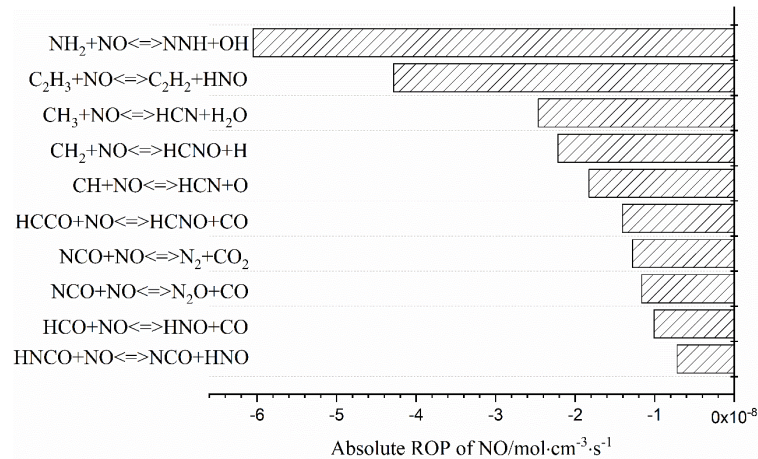
219
220 Fig.5 The influence of EAR_p on NO emission

221 Fig.5 shows the effects of EAR in the preheating zone on NO formation under different
 222 preheating and combustion temperatures. It was obvious that NO emission decreased first and then
 223 increased with the increase of EAR_p, even under different preheating temperatures and combustion
 224 temperatures. the NO emission achieved its lowest value when EAR_p was around 0.4.

225 For the experiments conducted in the single preheating chamber, the lowest NO in the outlet
 226 of preheating zone was achieved in EAR_p=0.1 (Wang, S. et al., 2020). However, for the preheating-
 227 combustion process, the lowest NO in the outlet of combustion chamber was achieved in EAR_p=0.4.

228 The shift of the optimized EAR_p to a higher level indicated that the optimization for NO formation
229 in single preheating process would not work in the whole preheating-combustion process. The main
230 reason was the continue conversion of nitrogen containing species in preheated fuel. The overall
231 EAR was kept constant as 1.2. Thus, the newly provided oxidizer for combustion of preheated fuel
232 of $EAR_p=0.2,0.4,0.6$ was $EAR_c=1.0,0.8,0.6$, respectively. When preheated fuel got into combustion
233 chamber, it met the combustion air and the nitrogen containing species continued to convert.
234 Especially for the condition of $EAR_p=0.2$, the remained HCN in preheated gas was oxidized quickly
235 once encountering oxygen. Thus, the chance to form NO from HCN and char-N in lower EAR_p
236 would be greater than that in high EAR_p due to the higher partial pressure of oxygen. Max et al.
237 (Weidmann et al., 2016) also indicated that the contribution of NO from char-N and HCN increases
238 with increasing available oxygen. In this study, the final NO achieved its lowest value at $EAR_p=0.4$,
239 with NO reduction efficiency of 60.38%. Under such condition, volatile-N was mainly converted in
240 the preheating stage under an oxygen deficient atmosphere (Wang, S. et al., 2020). Thus, the
241 conversion of char-N will contribute nearly 40% of NO. This is in line with the findings of Glarborg
242 (Glarborg et al., 2003; Glarborg et al., 2018) and Pohl (Pohl and Sarofim, 1977). Both reported that
243 60-80% of NO during bituminous coal combustion could be attributed to the conversion of volatile-
244 N, whereas the other 20-40% of NO is typically from char-N. Therefore, it can be concluded that
245 preheating-combustion process can effectively control NO emission from volatile-N (Ouyang et al.,
246 2020). Moreover, the combustion of preheated fuel can be integrated with other technologies, such
247 as air staging and MILD combustion, to further reduce the NO from char-N (Liu et al., 2015a; Liu
248 et al., 2014; Liu et al., 2015b).

261 increased under oxygen deficient conditions.



262

263

264

Fig.8 Absolute ROP of NO for different radicals at 0.2 s
(T_p=1573 K, T_c=1473 K, EAR_p=0.4, EAR_c=0.8)

265

Furthermore, the ROP analysis could illuminate the main reactions and species that played a

266

major role in NO formation and destruction. The analysis showed that NH₂ played a dominate role

267

in NO destruction, accounting for nearly 30%, as presented in Fig.8. In addition, a significant part

268

of NO was consumed by hydrocarbon radicals (C_iH_j), such as CH₃+NO, CH₂+NO and CH+NO,

269

which was consistent with the results of experiment conducted by Degaut (Dagaut and Lecomte,

270

2003). Other nitrogen-containing compounds, such as NCO and HNCO, could also reduce NO, but

271

the influence was slight.

272

4. Conclusion

273

In this work, NO emission characteristics during PC preheating-combustion process were

274

investigated using two series connected drop tube furnaces, and kinetic modeling of this process

275

was also conducted to better understand NO formation and destruction. The main conclusions are

276

as follows:

277

1) Increasing the temperature and prolonging the residence time in the preheating zone were

278

beneficial to the release and reduction of coal-N and the interaction between char-N and nitrogen

279

containing gases, which enhances the NO reduction potential of preheating-combustion process.

280

2) With an increase of excess air ratio (EAR) in the preheating zone, the NO emission first

281

decreased and then increased. An optimal EAP in preheating zone was identified at 0.4,

282 correspondingly, the lowest NO emission was 223 mg·m⁻³.

283 3) The results of kinetic modeling, which considered both homogeneous and heterogeneous
284 effects, showed an ability to reproduce the experimental results. Rate of production analysis
285 indicated that the importance of main radicals on NO destruction followed the sequence: NH₂> C₂H₅>
286 HCCO>NCO>HCO.

287

288 **Acknowledgements**

289 The present work was supported by National Natural Science Foundation of China (No.
290 51776161).

291

292 **References**

- 293 Bai, W., Li, H., Deng, L., Liu, H., Che, D., 2014. Air-Staged Combustion Characteristics of Pulverized
294 Coal under High Temperature and Strong Reducing Atmosphere Conditions. *Energ Fuel* 28(3), 1820-
295 1828.
- 296 Bryan, B., Nester, S., Rabovitser, J., Wohadlo, S., 2005. Methane de-NOX for Utility PC Boilers. Institute
297 Of Gas Technology.
- 298 Chernetskiy, M., Dekterev, A., Chernetskaya, N., Hanjalić, K., 2018. Effects of reburning mechanically-
299 activated micronized coal on reduction of NOx: Computational study of a real-scale tangentially-fired
300 boiler. *Fuel* 214, 215-229.
- 301 Dagaut, P., Lecomte, F., 2003. Experiments and kinetic modeling study of NO-reburning by gases from
302 biomass pyrolysis in a JSR. *Energ Fuel* 17(3), 608-613.
- 303 Glarborg, P., Jensen, A.D., Johnsson, J.E., 2003. Fuel nitrogen conversion in solid fuel fired systems.
304 *Prog. Energy Combust. Sci.* 29(2), 89-113.
- 305 Glarborg, P., Miller, J.A., Ruscic, B., Klippenstein, S.J., 2018. Modeling nitrogen chemistry in
306 combustion. *Prog. Energy Combust. Sci.* 67, 31-68.
- 307 Hashemi, H., Hansen, S., Toftegaard, M.B., Pedersen, K.H., Jensen, A.D., Dam-Johansen, K., Glarborg,
308 P., 2011. A Model for Nitrogen Chemistry in Oxy-Fuel Combustion of Pulverized Coal. *Energy & Fuels*
309 25(10), 4280-4289.
- 310 He, R., Suda, T., Takafuji, M., Hirata, T., Sato, J.i., 2004. Analysis of low NO emission in high
311 temperature air combustion for pulverized coal. *Fuel* 83(9), 1133-1141.
- 312 Hu, L., Zhang, Y., Chen, D., Fang, J., Zhang, M., Wu, Y., Zhang, H., Li, Z., Lyu, J., 2019. Experimental
313 study on the combustion and NOx emission characteristics of a bituminous coal blended with semi-coke.
314 *Appl. Therm. Eng.* 160, 113993.
- 315 LeBlanc, J., Quanci, J., Castaldi, M.J., 2017. Investigating Secondary Pyrolysis Reactions of Coal Tar
316 via Mass Spectrometry Techniques. *Energ Fuel* 31(2), 1269-1275.
- 317 Liu, C., Hui, S., Pan, S., Wang, D., Shang, T., Liang, L., 2015a. The influence of air distribution on gas-
318 fired coal preheating method for NO emissions reduction. *Fuel* 139, 206-212.
- 319 Liu, C., Hui, S., Pan, S., Zou, H., Zhang, G., Wang, D., 2014. Experimental Investigation on NOx
320 Reduction Potential of Gas-Fired Coal Preheating Technology. *Energ Fuel* 28(9), 6089-6097.

321 Liu, C., Hui, S., Zhang, X., Wang, D., Zhuang, H., Wang, X., 2015b. Influence of type of burner on NO
322 emissions for pulverized coal preheating method. *Appl Therm Eng* 85, 278-286.

323 Liu, W., Ouyang, Z.Q., Cao, X.Y., Nao, Y.J., 2018. Experimental Research on Flameless Combustion
324 with Coal Preheating Technology. *Energ Fuel* 32(6), 7132-7141.

325 Ma, L., Fang, Q., Yin, C., Wang, H., Zhang, C., Chen, G., 2019. A novel corner-fired boiler system of
326 improved efficiency and coal flexibility and reduced NO_x emissions. *Applied Energy* 238, 453-465.

327 Molina, A., Murphy, J.J., Winter, F., Haynes, B.S., Blevins, L.G., Shaddix, C.R., 2009. Pathways for
328 conversion of char nitrogen to nitric oxide during pulverized coal combustion. *Combustion and Flame*
329 156(3), 574-587.

330 Niksa, S., 2019a. Predicting nitrogen release during coal tar decomposition. *P Combust Inst* 37(3), 2765-
331 2772.

332 Niksa, S., 2019b. Simulating volatiles conversion in dense burning coal suspensions. 1. Validation of
333 chemical reaction mechanisms. *Fuel* 252, 821-831.

334 Niu, Y., Shang, T., Zeng, J., Wang, S., Gong, Y., Hui, S.e., 2017. Effect of Pulverized Coal Preheating on
335 NO_x Reduction during Combustion. *Energ Fuel* 31(4), 4436-4444.

336 Ouyang, Z., Ding, H., Liu, W., Cao, X., Zhu, S., 2020. Effect of the Primary Air Ratio on Combustion of
337 the Fuel Preheated in a Self-preheating Burner. *Combustion Science and Technology*, 1-18.

338 Ouyang, Z.Q., Liu, W., Man, C.B., Zhu, J.G., Liu, J.Z., 2018a. Experimental study on combustion, flame
339 and NO_x emission of pulverized coal preheated by a preheating burner. *Fuel Process. Technol.* 179, 197-
340 202.

341 Ouyang, Z.Q., Liu, W., Zhu, J.G., 2018b. Flameless combustion behaviour of preheated pulverized coal.
342 *Can. J. Chem. Eng.* 96(5), 1062-1070.

343 Ouyang, Z.Q., Liu, W., Zhu, J.G., Liu, J.Z., Man, C.B., 2018c. Experimental research on combustion
344 characteristics of coal gasification fly ash in a combustion chamber with a self-preheating burner. *Fuel*
345 215, 378-385.

346 Ouyang, Z.Q., Zhu, J.G., Lu, Q.G., 2013. Experimental study on preheating and combustion
347 characteristics of pulverized anthracite coal. *Fuel* 113, 122-127.

348 Pohl, J.H., Sarofim, A.F., 1977. Devolatilization and oxidation of coal nitrogen, Symposium
349 (International) on Combustion. Elsevier, pp. 491-501.

350 Rabovitser, J., Bryan, B., Knight, R., Nester, S., Wohadlo, S., Tumanovsky, A.G., Tolchinsky, E.N.,
351 Verbovetsky, E.H., Lisauskas, R., Beittel, R., 2003. Development and testing of a novel coal preheating
352 technology for NO_x reduction from pulverized coal-fired boilers. *Gas* 1(2), 4.

353 Rabovitser, J., Bryan, B., Wohadlo, S., Nester, S., Vaught, J., Tartan, M., Szymanski, L., Glickert, R.,
354 2007. Development of METHANE de-NO_x Reburn Process for Wood Waste and Biomass Fired Stoker
355 Boilers-Final Report-METHANE de-NO_x Reburn Technology Manual. Gas Technology Institute, Des
356 Plaines, IL 60018.

357 Society, C.E.R., 2020. China Energy Development Report 2020. China Energy Research Society, Beijing:
358 Social Sciences Academic Press.

359 Song, M., Huang, Q., Niu, F., Li, S., 2020. Recirculating structures and combustion characteristics in a
360 reverse-jet swirl pulverized coal burner. *Fuel* 270, 117456.

361 Taniguchi, M., Kamikawa, Y., Okazaki, T., Yamamoto, K., Orita, H., 2010. A role of hydrocarbon
362 reaction for NO_x formation and reduction in fuel-rich pulverized coal combustion. *Combustion and*
363 *Flame* 157(8), 1456-1466.

364 Taniguchi, M., Kamikawa, Y., Tatsumi, T., Yamamoto, K., 2011. Staged combustion properties for

365 pulverized coals at high temperature. *Combustion and Flame* 158(11), 2261-2271.

366 Taniguchi, M., Kamikawa, Y., Tatsumi, T., Yamamoto, K., Kondo, Y., 2012. Relationships between Gas-
367 Phase Stoichiometric Ratios and Intermediate Species in High-Temperature Pulverized Coal Flames for
368 Air and Oxy-Fuel Combustions. *Energy Fuel* 26(8), 4712-4720.

369 Tian, Y., Xie, K., Zhu, S., Fletcher, T.H., 2001. Simulation of coal pyrolysis in plasma jet by CPD model.
370 *Energy Fuel* 15(6), 1354-1358.

371 Ulusoy, B., Lin, W., Karlström, O., Li, S., Song, W., Glarborg, P., Dam-Johansen, K., Wu, H., 2019.
372 Formation of NO and N₂O during Raw and Demineralized Biomass Char Combustion. *Energy & Fuels*
373 33(6), 5304-5315.

374 Wang, S., Niu, Y., Li, T., Wang, D., Hui, S.e., 2020. Experimental and kinetic study on the transformation
375 of coal nitrogen in the preheating stage of preheating-combustion coupling process. *Fuel* 275, 117924.

376 Wang, Y., Zhou, Y., Bai, N., Han, J., 2020. Experimental investigation of the characteristics of NO_x
377 emissions with multiple deep air-staged combustion of lean coal. *Fuel* 280, 118416.

378 Weidmann, M., Honoré, D., Verbaere, V., Boutin, G., Grathwohl, S., Godard, G., Gobin, C., Kneer, R.,
379 Scheffknecht, G., 2016. Experimental characterization of pulverized coal MILD flameless combustion
380 from detailed measurements in a pilot-scale facility. *Combust Flame* 168, 365-377.

381 Wu, X., Fan, W., Ren, P., Chen, J., Liu, Z., Shen, P., 2019. Interaction between volatile-N and char-N and
382 their contributions to fuel-NO during pulverized coal combustion in O₂/CO₂ atmosphere at high
383 temperature. *Fuel* 255, 115856.

384 Zhu, G., Gong, Y., Niu, Y., Wang, S., Lei, Y., Hui, S.e., 2021. Study on NO_x emissions during the
385 coupling process of preheating-combustion of pulverized coal with multi-air staging. *Journal of Cleaner*
386 *Production* 292, 126012.

387 Zhu, S.-J., Lyu, Q.-G., Zhu, J.-G., Li, J.-R., 2018. NO emissions under pulverized char MILD combustion
388 in O₂/CO₂ preheated by a circulating fluidized bed: Effect of oxygen-staging gas distribution. *Fuel*
389 *Process. Technol.* 182, 104-112.

390

391

392 **Supplementary file**

393

394 **Experimental and kinetic studies on NO emission during pulverized coal preheating-**

395 **combustion process with high preheating temperature**

396 Shuai Wang ^a, Guangqing Zhu ^a, Yanqing Niu ^{a,*}, Yiyu Ding ^b, Shi'en Hui ^a

397 ^a State Key Laboratory of Multiphase Flow in Power Engineering, School of Energy and Power

398 Engineering, Xi'an Jiaotong University, Xi'an 710049, P. R. China

399 ^b Department of Energy and Process Engineering, Faculty of Engineering, NTNU — Norwegian

400 University of Science and Technology, Trondheim, Norway

401

402 Input conditions for kinetic modeling in Chemkin-Pro were provided for the reproduction of

403 the numerical results in this paper in Table S1.

404 **Table S1 Detailed input parameters for Chemkin-Pro**

specie s	input value (L·min ⁻¹)	
	Inlet I	Inlet II
N ₂	4.86;4.815;4.771;4.727;4.683;4.595;4.507; 4.332 (EAR _p =0; 0.1; 0.2; 0.3; 0.4; 0.6; 0.8; 1.2)	4.473;4.517;4.439;4.605;4.648;4.737;4. 824;5 (EAR _c =1.2; 1.1; 1.0; 0.9; 0.8; 0.6; 0.4; 0)
O ₂	0;0.043;0.878;0.132;0.176;0.263;0.351;0.5 27 (EAR _p =0; 0.1; 0.2; 0.3; 0.4; 0.6; 0.8; 1.2)	0.527;0.483;0.561;0.395;0.351;0.263;0. 176;0 (EAR _c =1.2; 1.1; 1.0; 0.9; 0.8; 0.6; 0.4; 0)
HCN	0.004052	0
CO	0.015321	0
CH ₄	0.038375	0
H ₂ O	0.055556	0
CO ₂	0.008886	0
C ₂ H ₆	0.0182	0
Char	0.000704	0

405

406

407

408

409